Journal of Zhejiang University-SCIENCE A (Applied Physics & Engineering) 2022 23(5):388-404
www.jzus.zju.edu.cn; www.springer.com/journal/11582
E-mail: jzus_a@zju.edu.cn

Research Article

https://doi.org/10.1631/jzus.A2100448

Numerical study on ethylene-air continuous rotating detonation in annular combustors with different widths

Wei-jie FAN[1], Wei-dong LIU[1]✉, Hao-yang PENG[1]✉, Shi-jie LIU[1], Jian SUN[2]

[1]*Science and Technology on Scramjet Laboratory, College of Aerospace Science and Technology, National University of Defense Technology, Changsha 410073, China*
[2]*State Key Laboratory of Aerospace Dynamic, Satellite Control Center, Xi'an 710043, China*

Abstract: To investigate the impact of combustor width on continuous rotating detonation (CRD) fueled by ethylene and air, a series of 3D simulations are conducted by changing the inner cylinder radius of an annular combustor while retaining the same outer cylinder radius. The results show that the CRD wave propagates more steadily and faster as the combustor width increases. The high-temperature zone at the backward-facing step preheats the propellants and contributes to the steady propagation of the CRD wave in 25- and 30-mm wide combustors. The highest and the lowest velocities are obtained in the 30- and 15-mm wide combustors at, respectively, 1880.27 and 1681.01 m/s. On the other hand, the average thrust decreases as the combustor width increases. The highest thrust is obtained in the 15-mm wide combustor while the lowest is in the 30-mm wide combustor, at 758.06 and 525.93 N, respectively. Nevertheless, the thrust is much more stable in the 25- and 30-mm wide combustors than in the 15- and 20-mm wide combustors.

Key words: Continuous rotating detonation (CRD); Ethylene-air; Combustor width; Propagation mode; Propulsive performance

1 Introduction

At present, the engines of aerospace propulsion systems usually work in the deflagration combustion mode. After much research-led development, the propulsive performance of these systems has almost reached its maximum theoretical value. Therefore, a new propulsion system using a different combustion mode has become an important issue. In the past decade, much research has centered on another combustion mode, detonation, because of its high heat release rate and thermodynamic efficiency (Bykovskii and Vedernikov, 1996; Stewart and Kasimov, 2006). In general, detonation-based engines in aerospace engineering applications can be divided into various categories including the pulse detonation engine (PDE) (Nikitin et al., 2009), the oblique detonation engine (ODE) (Fang et al., 2017), and the continuous rotating detonation engine (CRDE) (Lin et al., 2015; Sun et al., 2018a). Because CRDE can work in a broad range of flight conditions and produce a reasonably stable thrust with a compact engine structure, it has received a lot of attention in the field of propulsion research.

In the past two decades, extensive investigations on the working processes of CRDE have been conducted in annular combustors, such as the initiation (Bykovskii et al., 2007; Liu et al., 2013; Yang et al., 2016), the propagation modes (Lin et al., 2015; Liu et al., 2015; Sun et al., 2019), and the propulsive performance (Yi et al., 2011; Tang et al., 2015; Yao et al., 2017; Sun et al., 2018b). However, most of these investigations focused on a hydrogen CRDE due to the high chemical activity and detonation ability of hydrogen. However, considering both practicability and safety in engineering applications, hydrocarbon fuels, especially kerosene, may be superior to hydrogen for CRDE. At present, it is still hard to obtain stable liquid kerosene-air continuous rotating detonation (CRD) in the annular combustor owing to its low chemical activity and detonation ability (Kindracki,

✉ Wei-dong LIU, wdliu@nudt.edu.cn
Hao-yang PENG, penghaoyang@nudt.edu.cn
Wei-jie FAN, https://orcid.org/0000-0002-4766-5494

Received Sept. 12, 2021; Revision accepted Dec. 7, 2021;
Crosschecked Mar. 22, 2022

2015). Even with the addition of hydrogen and oxygen, the performance of liquid kerosene CRD is still quite poor. Bykovskii et al (2006a) experimentally investigated liquid kerosene-air CRD in an annular combustor with a 16.5-mm wide channel. The results showed that the CRD wave was hardly detonated unless the mass fraction of oxygen in the oxidant was higher than 50%. Le Naour et al. (2017) tried to establish a liquid kerosene detonation regime in an annular combustor with a 25-mm wide channel. Liquid kerosene CRD was successfully established due to the addition of hydrogen. However, the CRD wave propagated at a low velocity of about 1000 m/s and the velocity deficit was quite large. As the fuel composition changes from hydrogen to liquid kerosene, the chemical activity and detonation ability decrease significantly. The transition investigations of CRD fueled by hydrocarbons with moderate chemical activity help to a better understanding of liquid kerosene CRD and accelerate the application of CRDE in engineering.

Ethylene is one of the main components of kerosene pyrolysis products, with a higher chemical activity than kerosene but lower than hydrogen. In recent years, studies on ethylene CRD have been carried out in annular combustors (George et al., 2015; Cho et al., 2016; Wilhite et al., 2016; Andrus et al., 2017; Peng et al., 2019b). George et al. (2015) experimentally investigated ethylene-air CRD in an annular combustor and observed the single-wave propagation mode of the CRD wave. However, the highest propagation velocity of the CRD wave was only 850 m/s with severe propagation instability. Wilhite et al. (2016) carried out a set of ethylene-air CRD experiments in a 13.1-mm wide annular combustor and found the CRD wave could only be achieved with a limited range of equivalence ratios and mass flow rates. Cho et al. (2016) conducted ethylene-air CRD experiments in an annular combustor with a 7.6-mm wide channel and observed detonation waves propagated in a weak counter-rotating mode with an average velocity of (994±43) m/s. Andrus et al. (2017) experimentally studied the mixing effects on ethylene-air CRD in an annular combustor with a 23-mm wide gap. The CRD wave propagated at a velocity near the speed of sound and suffered a great velocity deficit even under the premixed supply condition. Peng et al. (2019b) performed a set of ethylene-air CRD experiments with the extra addition of hydrogen and oxygen in the racetrack-like combustor. The realized CRD wave propagated in a counter-rotating mode with a great velocity deficit. All in all, obtaining stable ethylene-air CRD in the annular combustor with a low velocity deficit is still challenging and needs further study.

To enhance the propagation performance of the ethylene-air CRD, new combustor configurations of CRDE are proposed, including the hollow combustor and the cavity-based annular combustor. Anand et al. (2018) investigated the ethylene-air CRD mechanics in a hollow combustor by using two different injection schemes. During stable propagation, the velocity of the CRD wave could reach about 95% of the Chapman-Jouguet (C-J) velocity. Peng et al. (2018) obtained a stable single-wave mode of ethylene-air detonation wave in the hollow combustor and the detonation wave could rotate with a velocity as high as 1915.40 m/s. Wang et al. (2018) also experimentally proved that the ethylene-air CRD was feasible in such a combustor. There was only one CRD wave rotating in the combustor under the operating conditions and the wave generally propagated at above 80% of the C-J velocity. Compared with the annular combustor, a more stable ethylene-air CRD was readily achieved in the hollow combustor. However, some deficiencies in the propulsive performance of the hollow combustor were found, which mainly resulted from the divergent flow (Tang et al., 2015) and from imperfect detonation combustion (Kawasaki et al., 2019). The cavity-based annular combustor is a novel kind of CRDE scheme put forward by Peng's team (Peng et al., 2019a, 2021; Liu et al., 2020). By installing a cavity at the inner cylinder of the annular combustor, the width of the combustor increased and the combustion organization was improved. As a result, the operating range of the ethylene-air CRD was increased and the propagation velocity of the detonation wave increased to some extent. However, the velocity deficit was still in the range of 30% to 40% of the C-J velocity, which was high. The combustor configuration has great effects on the operation of the CRD and the requirements for stable propagation and the optimization of efficient propulsive performance deserve further study.

Only a few simulations on ethylene detonation were carried out because of its low chemical activity and the great difficulty in initiation (Khokhlov et al., 2004; Yungster and Radhakrishnan, 2005; Gottiparthi

et al., 2009; Schwer and Kailasanath, 2013; Fujii et al., 2017). The cellular detonation structures were analyzed using 1D (Yungster and Radhakrishnan, 2005) and 2D (Khokhlov et al., 2004; Gottiparthi et al., 2009) simulations. Ignoring the impacts of the combustor width and using 2D simulations, Schwer and Kailasanath (2013) analyzed the flow field and the specific impulse of a CRDE fueled by the ethylene-air mixture. Fujii et al. (2017) investigated the velocity of the ethylene-oxygen CRD wave by 2D simulations. Some information on the flow field and propagation characteristics of ethylene-air CRD was obtained. Fan et al. (2021) studied the propagation characteristics of ethylene-air CRD under different injection conditions by 2D simulations. The transition process of the detonation wave propagation mode was analyzed in detail. However, the combustor width was found to be key for realization of hydrocarbon CRD (Bykovskii et al., 2006b; Kawasaki et al., 2019). The propagation characteristics of the ethylene-air CRD wave and the propulsive performance of the CRDE with an enlarged annular combustor are still unclear. Thus, numerical investigation on the ethylene-air CRD with variation of the combustor width can contribute to pinpointing a self-sustaining mechanism.

In this study, the impact of the combustor width on the ethylene-air CRD is studied numerically by using 3D simulations. The propagation characteristics of the CRD wave and the propulsive performance of the CRDE are discussed. In addition, the self-sustaining mechanism of the CRD wave is analyzed. This study will deepen understanding of the ethylene-air CRD and give some guidance for the design of the combustor in a CRDE fed by hydrocarbon fuels.

2 Physical model and numerical method

2.1 Physical model

The cross-sectional schematic of the CRDE combustor under the premixed injection condition is shown in Fig. 1. A stoichiometric ethylene-air mixture is injected axially into the combustor through an annular slot. The throat width of the slot and the length of the combustor are 1.2 and 100 mm, respectively. The outer radius of the combustor is kept constant as 65 mm, while the inner radius of the cylinder is lowered from 50 to 35 mm at intervals of 5 mm. Thus,

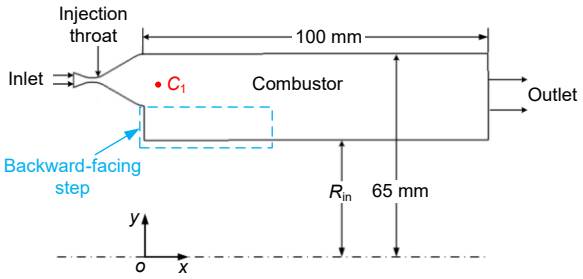

Fig. 1 Cross-sectional schematic of the CRDE combustor. R_{in} is the inner radius of the cylindrical combustor

the combustor width (W) varies from 15 to 30 mm at intervals of 5 mm. In addition, a pressure monitor point named C_1 is placed in the combustor with coordinates (5 mm, 57.5 mm, 0 mm) to record the pressure profile in the combustor caused by the CRD wave.

2.2 Numerical method

All cases in this investigation are solved by the commercial software ANSYS FLUENT, which is widely applied in the CRD research field (Sun et al., 2018a, 2018b, 2019). A stoichiometric ethylene-air mixture is injected at the inlet and the ideal gas law is used to calculate the density. Three-dimensional Reynolds-averaged Navier-Stokes (RANS) controlling equations are solved by the transient implicit density-based solver. The inviscid flux vector is evaluated by Roe's flux-difference splitting (Roe-FDS) method. For spatial discretization, the cell-based least squares method is used to compute the gradient, and the second-order upwind scheme is applied for flow, turbulent kinetic energy, and specific dissipation rate. The second-order implicit scheme is used for time stepping. The time step is fixed as 0.1 μs and the instantaneous pressure at the monitor point is sampled at each time step to reconstruct the pressure record curves. The shear-stress transport (SST) k-ω turbulence model is employed to simulate the turbulent flow. The laminar finite rate reaction model and the reaction rate constants are determined by the Arrhenius formulation, i.e.,

$$k_f = AT^b \exp\left(\frac{-E_a}{RT}\right), \tag{1}$$

where k_f is the reaction rate constant, A is the pre-exponential factor, T is the temperature, R is the gas constant, E_a is the activation energy, and b is the

temperature exponent. A reduced chemical mechanism (Baurle et al., 1998) treating three reactions with seven reacting species is applied, including nitrogen (N_2) as the seventh species. The leading edge of the backward-facing step is located at x=0 mm. To avoid flashback, the chemical reaction is artificially shut down in the upstream (zone of x<0 mm) and only occurs in the combustor (zone of x≥0 mm). Such reaction restriction has been generally adopted in simulations under premixed conditions (Schwer and Kailasanath, 2012; Sun et al., 2017). To further verify the chemical mechanism, a 1D detonation study using a grid size of 0.5 mm is conducted here. The domain is 2000-mm long and is filled with a stoichiometric ethylene-air mixture. The static pressure and static temperature of the combustible mixture are respectively 100 kPa and 300 K. Twenty monitor points at intervals of 100 mm are set along the line (x axis) to record the static pressure during the propagation process of the detonation wave. The pressure record curves and propagation velocities of the detonation wave are shown in Fig. 2. Based on the stable propagation process between 950 and 1950 mm, the average detonation propagation velocity is 1863 m/s with a 2.17% relative difference from the theoretical C-J velocity. This velocity difference is acceptable, and thus the reduced chemical mechanism is deemed reliable.

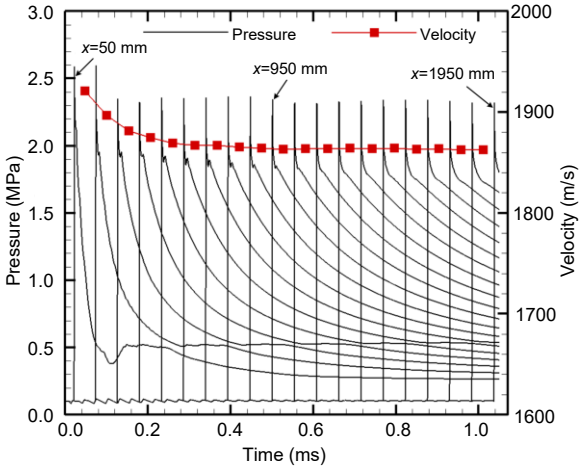

Fig. 2 Pressure record curves and propagation velocities of the 1D detonation

The mass flow inlet boundary condition is adopted at the mixture inlet. The total mass flow rate and the total temperature of the stoichiometric ethylene-air mixture are 800.31 g/s and 300 K, respectively. The pressure outlet condition boundary is used at the exit of the combustor and the backpressure is set to 100 kPa. All the walls are non-slip and adiabatic.

The computational domain is meshed with hexahedron cells using the commercial software ICEM CFD. When the research focuses on the main propagation characteristics and propulsive performance rather than the detailed structure of the CRD wave, grids with a size of 0.5 mm were widely used and reliable results could be obtained (Tang et al., 2015; Sun et al., 2018b). In this study, grids with an average axial size of 0.25 mm are used in the domain of 0≤x≤30 mm while grids with an average axial size of 0.50 mm are adopted in the remaining computational domain. The average size of grids is 0.50 mm in the radial and circumferential directions. To further confirm grid independence, some 2D simulations are carried out. The rectangular domain is 300-mm long and 100-mm wide and it is discretized by grids with the accuracy of 0.5, 0.25, and 0.125 mm correspondingly. A stoichiometric ethylene-air mixture is injected from the bottom boundary with a total pressure of 500 kPa and a total temperature of 300 K. The detonation products are discharged from the top boundary with a backpressure of 100 kPa. The two side borders are set as periodic boundaries which ensure that the detonation wave propagates continuously. As Fig. 3 displays, similar flow field structures are well captured by all three grids including the CRD wave, oblique shock wave, slip line, triple point, and fresh mixture layer. The results show that grids of the size of 0.5 mm are fine enough to obtain the basic flow field characteristics of a CRD wave. The grids used in this study are thought to obtain reliable results for ethylene-air CRD.

The initiation setup is demonstrated in Fig. 4, in which the black solid line and green solid line respectively indicate the locations of x=0 mm and x=10 mm. The preset flow field can be divided into three zones including combustible mixture zone (1) (marked in red), ignition zone (2) (marked in green), and downstream zone (3) (marked in blue). Zone (1) and zone (3) are both cylindrical in area and their axial coordinate ranges are respectively −18 mm≤x≤10 mm and 10 mm<x≤100 mm. Zone (2) is a fan-shaped area and its coordinates are 0≤x≤10 mm, −5 mm≤y≤5 mm, and z ranging from the corresponding inner wall to the outer wall. The detonation is expected to be ignited in

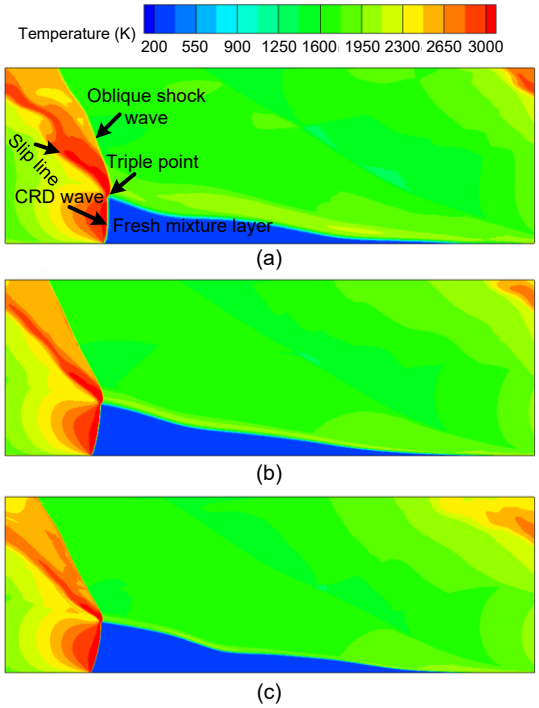

Fig. 3 Temperature contours of three grid sizes: (a) 0.50 mm; (b) 0.25 mm; (c) 0.125 mm

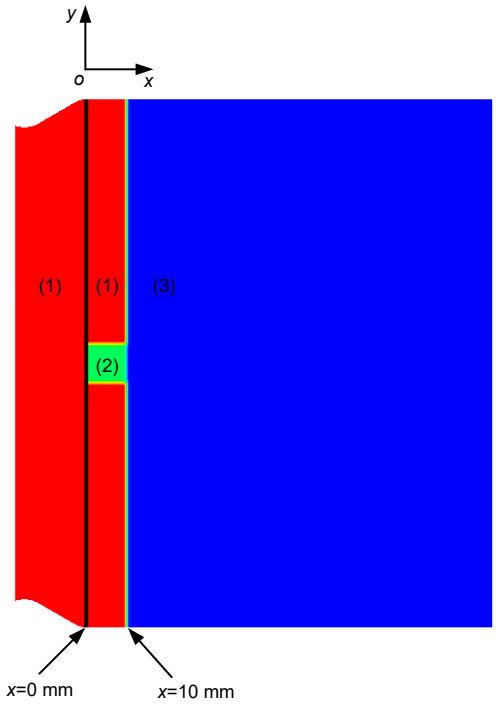

Fig. 4 Preset flow field in the initiation setup

zone (2) with high pressure (2000 kPa) and high tangential speed (2000 m/s). More detailed information about the preset flow field is listed in Table 1. The ignition zone with high pressure and tangential velocity is expected to ignite the combustible mixture and form the CRD wave.

Table 1 Detailed information of the preset flow field in the initiation setup

Zone	P (kPa)	T (K)	V (m/s)	Species
(1)	100	300	(100, 0, 0)	C_2H_4-air
(2)	2000	300	(0, 2000, 0)	H_2O
(3)	100	300	(100, 0, 0)	Air

3 Results and discussion

The stoichiometric ethylene-air CRD in combustors of different widths is simulated at a constant total mass flow rate of 800.31 g/s. The CRD wave propagation process shows great differences as the combustor width varies. In addition, the characteristics of the flow field are revealed by analyzing contours on axial slices and radial-azimuthal slices. Finally, the propulsive performances of different combustors are also quantitatively studied.

3.1 Effects of combustor width on the CRD wave propagation process

The propagation processes of the CRD wave in different combustors are analyzed in this section. When the CRD wave propagates circumferentially passing by the monitor point, the high pressure resulting from the CRD wave will be captured. The pressure curves obtained by the monitor point C_1 are shown in Fig. 5. The propagation processes of the CRD wave clearly vary with the different combustor widths.

When the combustor width is 15 mm, the propagation process of the CRD wave is quite unstable and the propagation mode changes many times over time, as shown in Fig. 5a. The propagation mode can be classified as either a single-wave mode, an unsteady multiple-wave mode, a co-rotating two-wave mode, or a co-rotating three-wave mode. In addition, the amplitude of the pressure peak varies greatly, which means the intensity of the CRD waves changes violently. To show the evolution of the CRD wave in the annular combustor more intuitively, cylindrical surfaces with a radius of 57.5 mm are unrolled into 2D surfaces colored by temperature contours as shown in

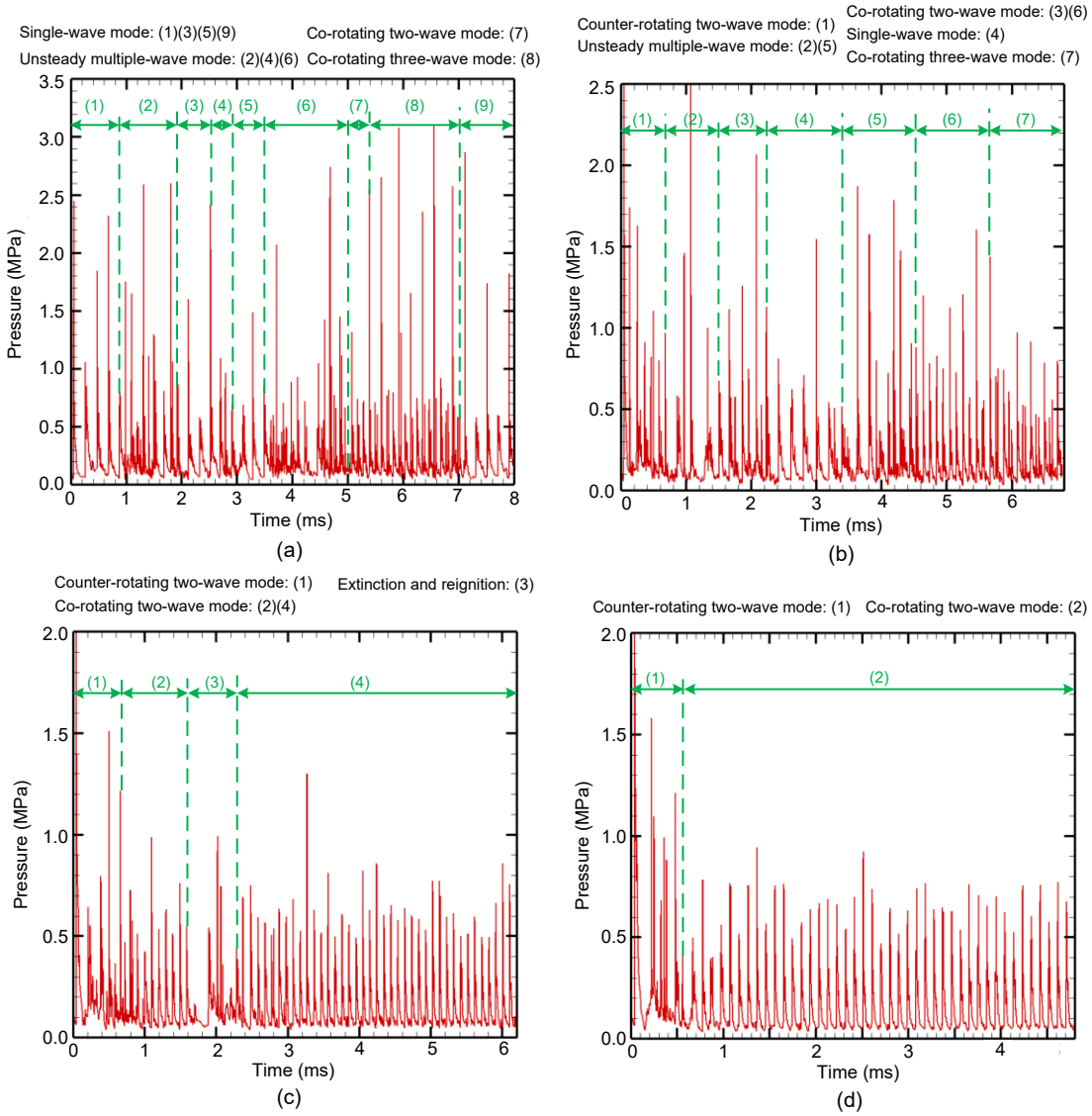

Fig. 5 Pressure record curves of monitor point C_1 in different combustors: (a) W=15 mm; (b) W=20 mm; (c) W=25 mm; (d) W=30 mm

Fig. 6. It can be seen that the preset ignition zone spreads unidirectionally along the tangential velocity direction, and then the combustible mixture is strongly compressed and ignited. At the time of 0.50 ms, the CRD wave is first established and it propagates in the single-wave mode, i.e., there is only one CRD wave propagating circumferentially in the combustor. However, this CRD wave cannot maintain a single-wave mode for long as the hot combustion product heats the fresh combustible mixture and induces a new detonation wave. As illustrated in Fig. 7, the hotspot behind the CRD wave induces two new CRD waves that propagate in opposite directions at the time of 1.00 ms. At the time of 1.04 ms, the induced CRD wave collides with the previous one resulting in a high-temperature and high-pressure zone. Then, the CRD waves decay into transmitted shock waves at the time of 1.06 ms. When there is enough fresh combustible mixture in front of the transmitted shock wave and the intensity of the shock wave is high enough to ignite the combustible mixture, the shock wave can re-evolve into a CRD wave, otherwise it will get extinguished as shown at the time of 1.10 ms. Due to the generation of a new CRD wave by the hotspot and the extinction of the CRD wave by the collision, there are multiple CRD waves propagating in an

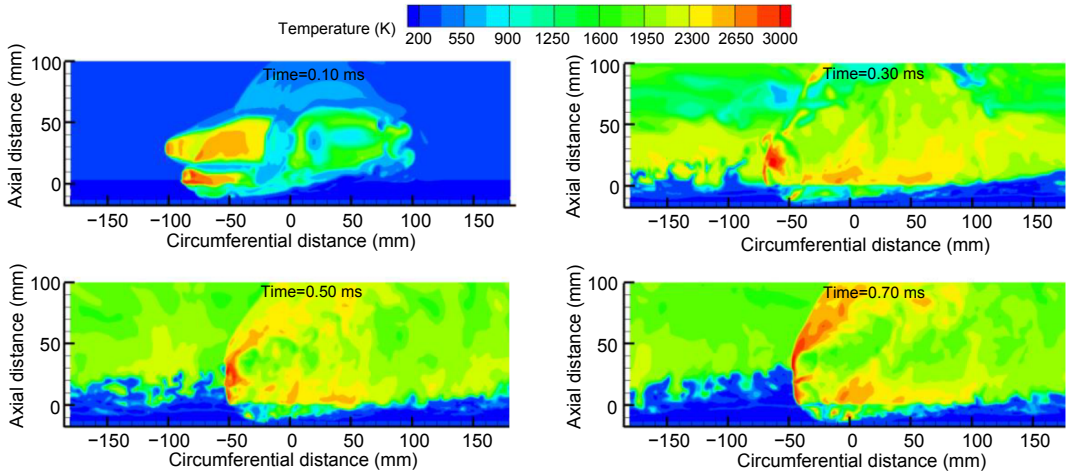

Fig. 6 Single-wave propagation mode after ignition (W=15 mm)

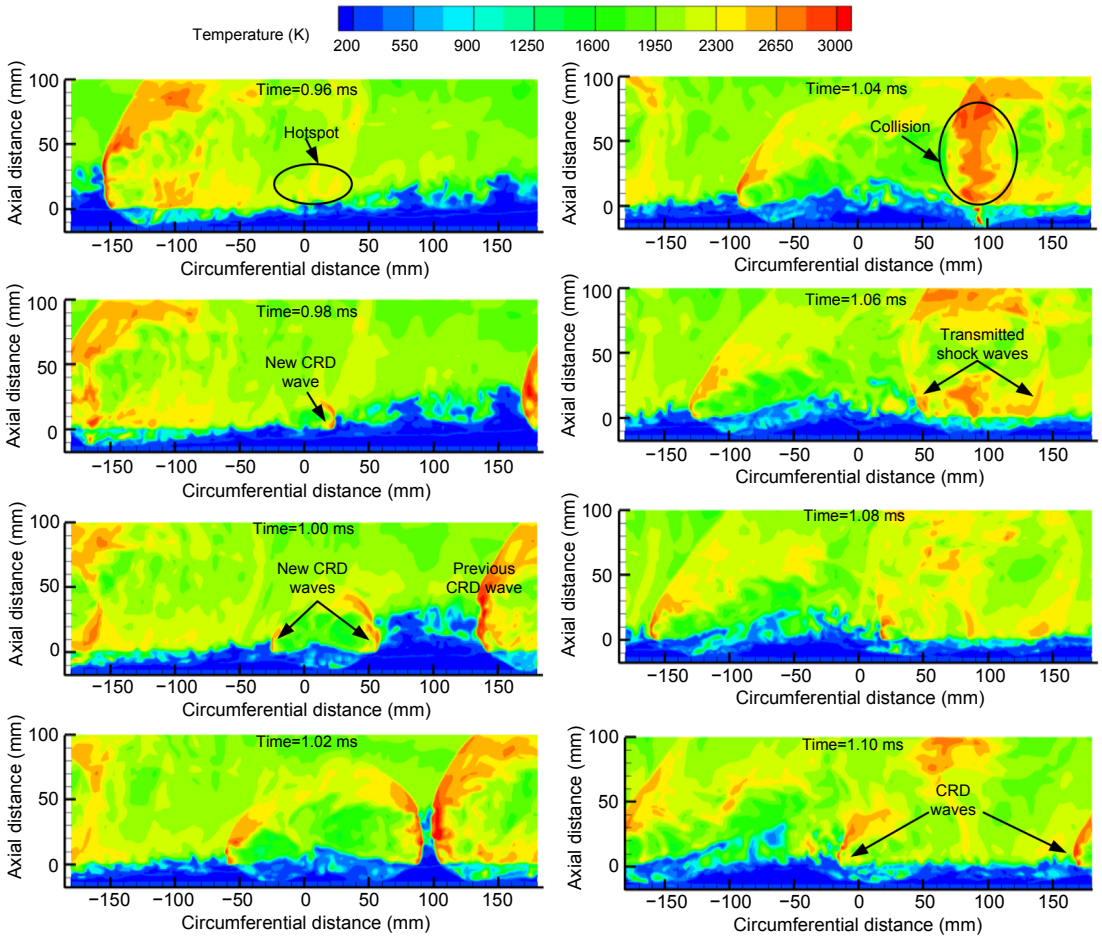

Fig. 7 Unsteady multiple-wave propagation mode (W=15 mm)

unsteady multiple-wave mode. This mode can be regarded as an intermediate mode of transition. After the adjustment in the unsteady multiple-wave mode, a co-rotating two-wave mode is observed in Fig. 8, i.e., two CRD waves propagate in the same direction in the combustor. Before long, the co-rotating two-wave mode may transform into a co-rotating three-wave mode as the hot combustion products induce another

new CRD wave. As Fig. 9 shows, the circumferential distance between the CRD waves on the left side is not long enough to establish a stable combustible mixture layer, which is mainly attributed to the high pressure behind the CRD waves blocking the injection of the fresh mixture. Soon afterwards, the induced CRD wave gets extinguished. For the same reason that the continuous propagation of the detonation wave is greatly affected by the refilled fresh mixture, the detonation wave propagates again in single-wave mode at the time of about 7.00 ms. However, the propagation mode of the CRD wave may change again in the subsequent propagation process. Above all, the propagation process of the CRD wave in the 15-mm wide combustor is unsteady.

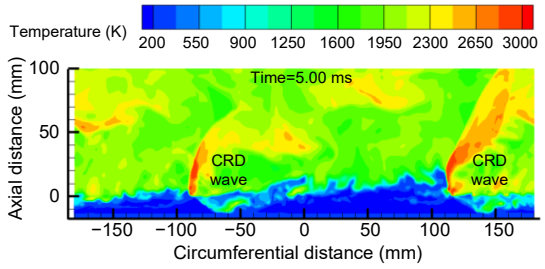

Fig. 8 Co-rotating two-wave mode (W=15 mm)

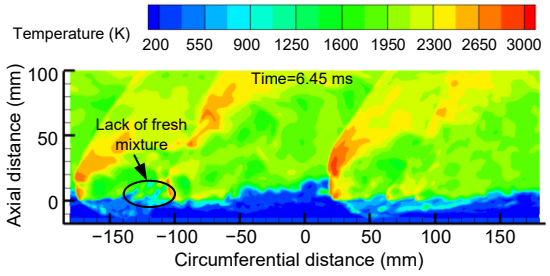

Fig. 9 Co-rotating three-wave mode (W=15 mm)

In the 20-mm wide combustor, the CRD wave still cannot sustainably maintain a stable propagation mode. Five kinds of propagation modes are observed including a counter-rotating two-wave mode, an unsteady multiple-wave mode, a single-wave mode, a co-rotating two-wave mode, and a co-rotating three-wave mode. Firstly, the ignition zone spreads to both sides and two counter-rotating CRD waves are formed as shown in Fig. 10. After the collision of the CRD waves, the propagation mode transforms into an unsteady multiple-wave mode. Affected by these unstable factors, including the unstable injection state

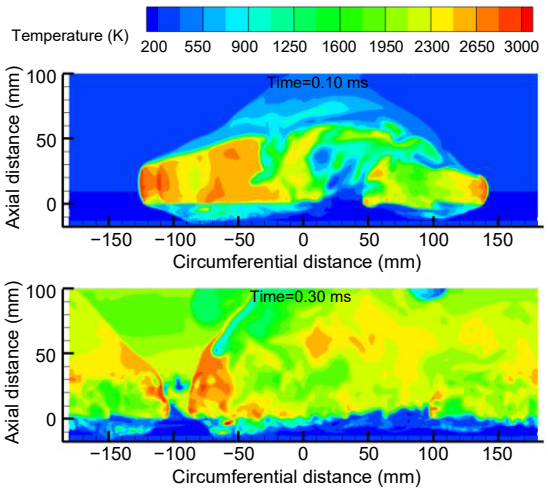

Fig. 10 Counter-rotating two-wave mode (W=20 mm)

of the premixed mixture and the induced combustion of the detonation product, the extinction and generation of the CRD wave occur from time to time. This causes frequent changes in the CRD wave propagation mode in the 20-mm wide combustor.

The instantaneous propagation modes of the CRD waves in the 25- and 30-mm wide combustors are carefully identified by an analysis both of the pressure record curves in Figs. 5c and 5d and of the unrolled 2D temperature contours as in Fig. 7. In the 25-mm wide combustor, the CRD waves propagate in counter-rotating two-wave mode after ignition. However, the mode changes into a co-rotating two-wave mode after the collision of the CRD waves. The extinction and reignition of the CRD waves are shown in Fig. 11. Due to the interaction between the CRD wave propagation and the injection of fresh mixture, the detonation waves get extinguished for lack of fresh mixture in front of the waves at the time of about 1.64 ms. After the combustible mixture layer is re-established and balanced, the CRD waves are reignited and finally propagate steadily in a co-rotating two-wave mode. For W=30 mm, the CRD waves propagate in co-rotating two-wave mode steadily and sustainably after a short adjustment in counter-rotating two-wave mode. As Fig. 12 displays, the propagation direction of the detonation waves in the steady propagation process is opposite to the initiation direction in the 25- and 30-mm wide combustors. After reignition or collision, newly generated detonation waves usually propagate in a direction where the combustible mixture is sufficient. Thus, the propagation direction of the CRD wave may get changed in the propagation process.

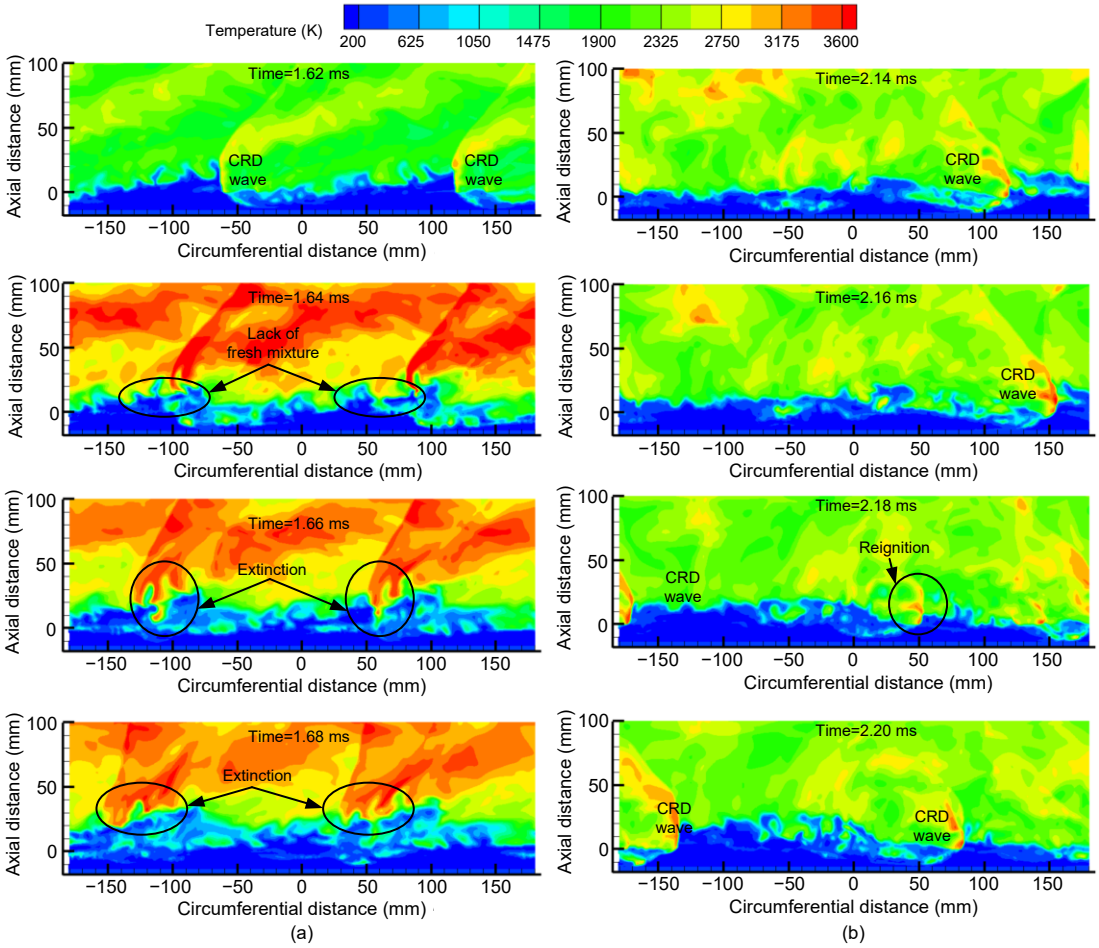

Fig. 11 Extinction (a) and reignition (b) of the CRD waves (W=25 mm)

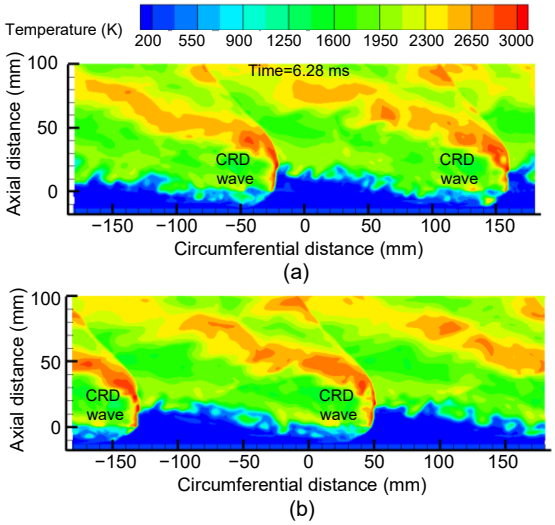

Fig. 12 Steady propagation of the CRD waves in the combustors with W=25 mm (a) and W=30 mm (b)

A similar phenomenon was also found and analyzed in (Sun et al., 2017).

In addition, the time interval required for the detonation wave to propagate in a cycle can be obtained by the pressure peaks of the pressure record curves. Combining those with the coordinates of the monitor point C_1, the instantaneous velocity of the detonation wave in a cycle can be calculated. Since there is reignition or extinction of the CRD wave in the counter-rotating two-wave mode and unsteady multiple-wave mode, the propagation velocity is hard to calculate in such modes. Therefore, only the velocities in steady propagation modes are taken into consideration, including the single-wave mode, the co-rotating two-wave mode, and the co-rotating three-wave mode. The average propagation velocity of the CRD wave, V_{CRD}, can be obtained (Sun et al., 2018a, 2018b, 2019). As Table 2 lists, the average propagation velocity increases with the increase in the combustor width. The highest velocity is obtained in the 30-mm wide combustor and reaches 1880.27 m/s, while the lowest

Table 2 Average propagation velocities of the CRD wave (V_{CRD}) in different combustors

W (mm)	V_{CRD} (m/s)
15	1681.01
20	1740.83
25	1838.49
30	1880.27

velocity is acquired in the 15-mm wide combustor at 1681.01 m/s.

From the above-mentioned discussions, the critical combustor width for the steady propagation of the stoichiometric ethylene-air CRD wave is found to be 25 mm in the tests under a constant mass flow rate of 800.31 g/s. When the combustor width is smaller than 25 mm, the CRD wave cannot propagate steadily in a single mode but it can self-sustain steadily in co-rotating two-wave mode when the combustor width is 25 or 30 mm. Moreover, the average propagation velocity of the CRD wave increases as the combustor width increases.

3.2 Effects of the combustor width on the flow field characteristics

To investigate the characteristics of the flow field in the combustors, the temperature contours on the x= 10 mm surfaces and the radial-azimuthal surfaces in front of the CRD wave are chosen for analysis. In addition, ethylene (C_2H_4) reacts with oxygen (O_2) to produce hydrogen (H_2) and carbon monoxide (CO) in the primary reaction (Baurle et al., 1998). The intermediate products are more chemically active than ethylene and may contribute to the steady propagation of the CRD wave and, therefore, the contours of the mass fraction of hydrogen (H_2) are also analyzed.

Fig. 13 shows the temperature contours and H_2 mass fraction contours on the x=10 mm surfaces of different combustors. As the propagation mode in the 15- and 20-mm wide combustors changes frequently, only the flow field in the co-rotating three-wave mode is chosen for analysis. As Fig. 13a shows, the fresh mixture layer forms a low-temperature zone in front of the CRD waves. Obviously, the detonation waves are non-uniformly distributed along the circumferential direction when the width is 15 or 20 mm. There is a greater interaction on the injection of fresh combustible mixture between two closer waves. The injection of the fresh mixture is more likely to be blocked by the high-pressure products as shown in Fig. 13b, and thus the mixture layer in front of the waves is quite short along the circumferential direction. For the lack of fresh mixture, the following CRD wave may get extinguished and the propagation mode of the CRD wave may be transformed. As the combustor width increases to 25 and 30 mm, the CRD waves in the combustors are evenly distributed along the circumferential direction with central angles of 179.0° and 178.3°, respectively. The long circumferential distance between the CRD waves allows the fresh mixture to be fully injected so that a long fresh mixture layer can be established. This contributes to the long-term stable propagation of the CRD waves. Fig. 13c illustrates the H_2 mass fraction contours in different combustors. Obviously, in the 15- and 20-mm wide combustors, hydrogen is mainly distributed in front of the CRD waves due to the chemical reactions caused by detonation. However, when the width is 25 or 30 mm, there is a large amount of hydrogen on the interface between the fresh mixture layer and the detonation product. The high-temperature detonation product induces the preliminary chemical reactions of the propellants, which produce high-activity intermediate products, such as hydrogen. The induced time and length of hydrogen are both shorter than those of ethylene, indicating that hydrogen has higher detonation ability than ethylene.

For a better understanding of the flow field along the axial direction, temperature contours and H_2 mass fraction contours on the radial-azimuthal surfaces in front of the CRD waves are also selected for analysis. When the combustor width is larger than 15 mm, a backward-facing step is formed at the forepart of the combustor due to the sudden expansion of the cross-sectional area of the channel there, as shown in Fig. 1. As Fig. 14a displays, a high-temperature zone filled with detonation product is formed at the backward-facing step especially in the 25- and 30-mm wide combustors. The residence phenomenon of the hot detonation products at the backward-facing step was also experimentally observed by Hsu et al. (2020) using megahertz-rate OH planar laser-induced fluorescence imaging. The high-temperature zone works as a pilot flame and preheats the freshly injected mixture. As a result, the induced length and time of the propellant are greatly reduced with higher initial temperature (Peng et al., 2019a). Moreover, the primary

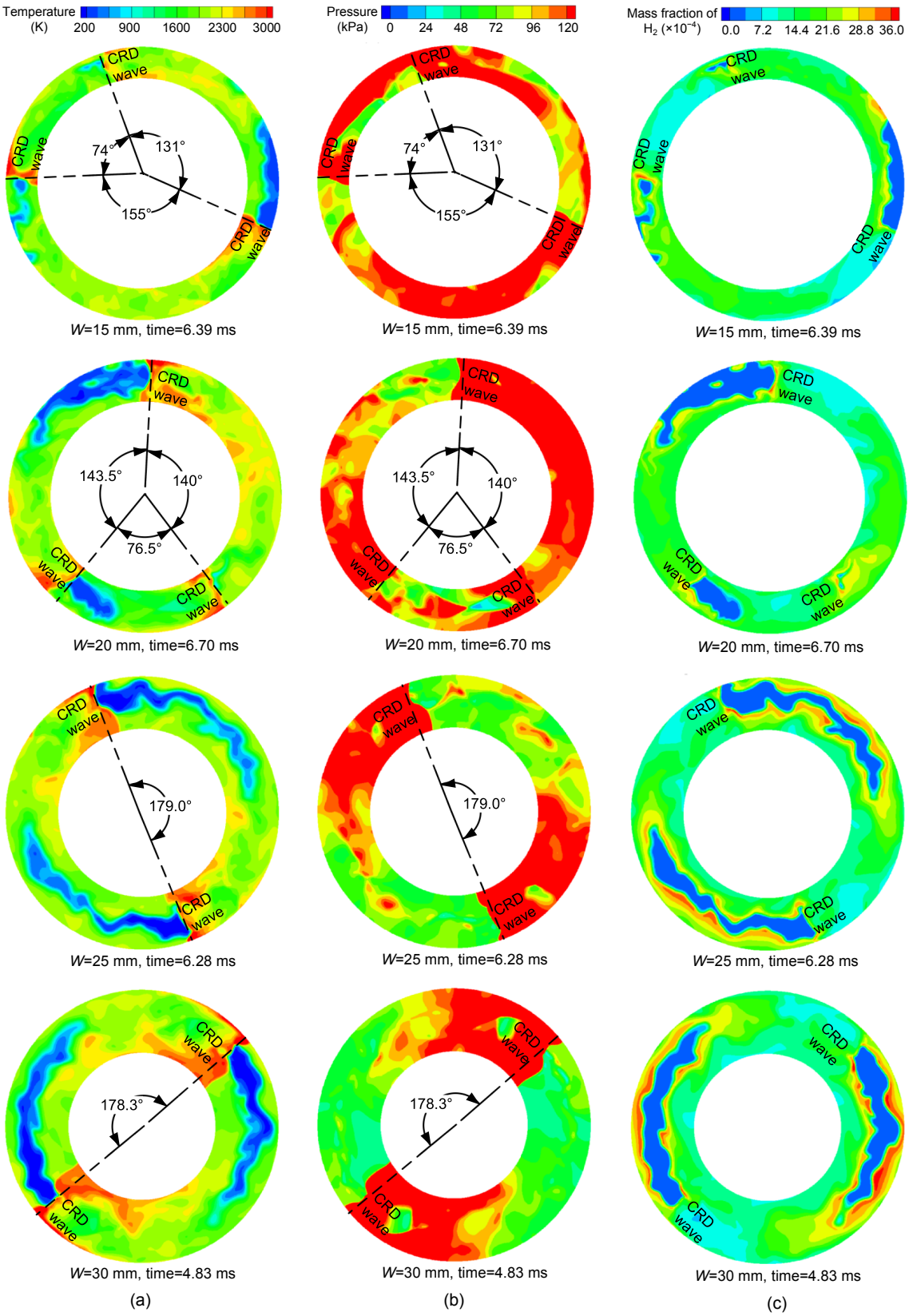

Fig. 13 Contours on the x=10 mm surfaces: (a) temperature contours; (b) pressure contours; (c) H_2 mass fraction contours

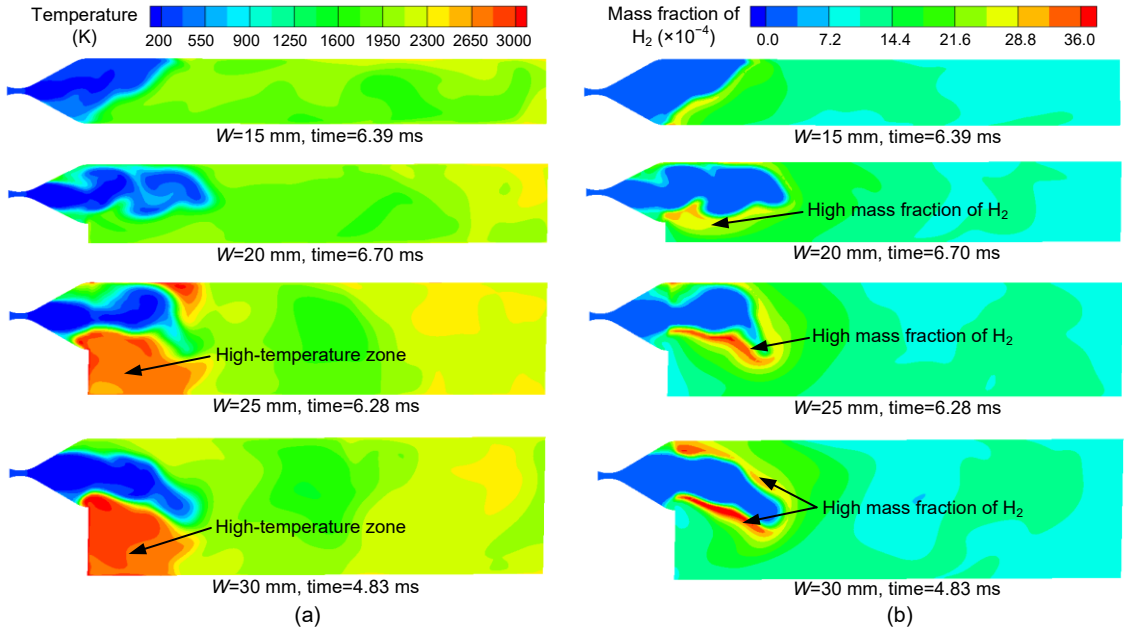

Fig. 14 Contours on the radial-azimuthal surfaces in front of the CRD waves: (a) temperature contours; (b) H_2 mass fraction contours

combustion products with high chemical activity, such as hydrogen, are produced on the interface between the accumulation layer of combustible mixture and the high-temperature zone, as Fig. 14b illustrates. The mass flow rates of ethylene and intermediate product hydrogen along the axial direction are calculated by

$$\dot{m}_i(x) = \iint \rho u \varphi_i \mathrm{d}y\mathrm{d}z, \tag{2}$$

where ρ is the density, u is the velocity along the x direction (axial direction), and φ_i represents the mass fraction of species i referring to ethylene or hydrogen.

As Fig. 15 shows, the mass flow rate of ethylene decreases as the axial distance increases. However, the distances that ethylene is advected downstream in different combustors are different. The ethylene is advected to the axial location of 20 mm in the 15-mm wide combustor but is transported further downstream to near the axial location of 30 mm in the other three combustors. The mass flow rate of hydrogen along the axial direction is plotted in Fig. 16. The mass flow rate of hydrogen firstly increases to a maximum value and then drops with some fluctuations as the axial distance increases. The increase results from the preheating effects of the hot detonation products on the fresh mixture, as mentioned above, while the drop is due to the consumption of the detonation wave. The

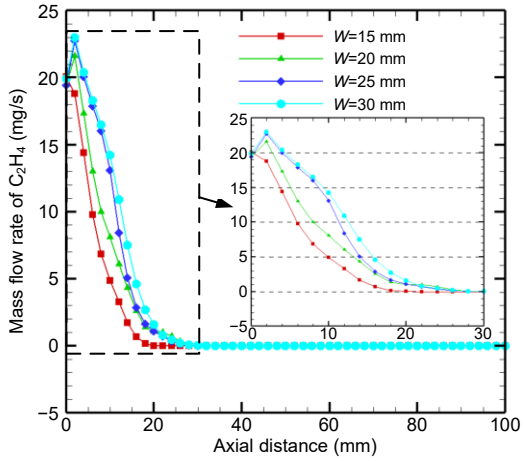

Fig. 15 Mass flow rates of ethylene along the axial distance

incomplete detonation leads to deflagration downstream and thus results in the fluctuation of the mass flow rate of hydrogen downstream. The maximum mass flow rate of hydrogen in the 15-mm wide combustor is significantly lower than that in the other three combustors. That is due to the more severe preheating effects of the hot detonation products at the backward-facing step in the other three combustors. Moreover, the maximum value of the mass flow rate of hydrogen in the 15-mm wide combustor is obtained at the axial location of 14 mm, while those in the other three combustors are obtained at the axial

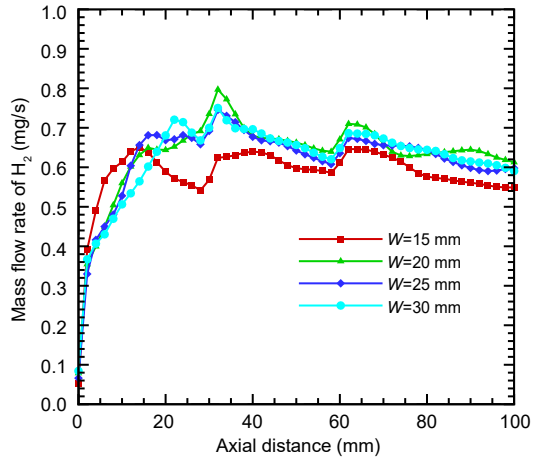

Fig. 16 Mass flow rates of hydrogen along the axial distance

location of 32 mm. Above all, the reactants and intermediate products can be transported further along the axial direction in the wider combustors, which establishes a suitable fresh mixture layer in front of the detonation wave. All these favorable factors contribute to the steady propagation of detonation waves in the wider combustors.

3.3 Effects of combustor width on the propulsive performance

Propulsive performance is of great importance in the CRDE design process. In this section, the effects of combustor width on the propulsive performance are analyzed. The thrust F can be calculated by Eq. (3), where A is the exit area of the combustor, p is the static pressure, and p_b is the ambient pressure which is set at 0.1 MPa. Moreover, the mass-average pressure and the mass-average axial velocity along the axial distance are calculated by Eqs. (4) and (5), respectively.

$$F(t)=\iint\left(\rho u^2+p-p_b\right)\mathrm{d}A, \tag{3}$$

$$\bar{p}(x)=\frac{\iint \rho up\mathrm{d}y\mathrm{d}z}{\iint \rho u\mathrm{d}y\mathrm{d}z}, \tag{4}$$

$$\bar{u}(x)=\frac{\iint \rho uu\mathrm{d}y\mathrm{d}z}{\iint \rho u\mathrm{d}y\mathrm{d}z}. \tag{5}$$

The thrust record curves of different combustors are illustrated in Fig. 17. In the 15- and 20-mm wide combustors, the thrust fluctuates widely, especially in the unsteady multiple-wave mode. In the co-rotating propagation mode, the number of detonation waves has little impact on the magnitude of the thrust. However, as Figs. 17a and 17b show, the extinction of the detonation wave may cause fluctuation of the thrust while an increase in the number of the detonation waves will not. As the combustor width increases to 25 and 30 mm, the thrust keeps quite stable with small fluctuations due to the steady propagation of the CRD waves in co-rotating two-wave mode.

Based on the thrust record curves, the average thrust and relative standard deviation (RSD) of the thrust of the different combustors are calculated and listed in Table 3. The average thrust decreases considerably from 758.06 to 525.93 N as the combustor width increases from 15 to 30 mm. Nevertheless, the RSD of the thrust is as high as 16.92% and 19.69% in the 15- and 20-mm wide combustors, respectively, while it is just 5.49% and 5.87% in the 25- and 30-mm wide combustors, respectively. This is beneficial by giving a steadier propagation process of the CRD wave in the 25- and 30-mm wide combustors. It can be inferred from Eq. (3) that the pressure at the exit of the combustor and the axial velocity both affect the thrust of the CRDE. The mass-average pressure and the mass-average axial velocity are plotted in Figs. 18 and 19, respectively. The pressure first rises and then falls sharply due to the quick heat release of the detonation and the rapid expansion behind the CRD wave, which occurs within 20-mm long axial distance at the forepart of the combustor. When the axial distance is larger than 20 mm, the pressure decreases slowly as the axial distance increases. The highest pressure is obtained in the 15-mm wide combustor due to the smallest cross-sectional area of the channel. It is worth noting that the pressure peak in the 25-mm wide combustor is much higher than that in the 20-mm wide combustor. This results from the more efficient detonation combustion in the 25-mm wide combustor as discussed in Section 3.2. Due to the larger volume of the combustor, the pressure behind the CRD wave in the 25-mm wide combustor drops more quickly than that in the 20-mm wide combustor. Unsurprisingly, the lowest pressure is obtained in the 30-mm wide combustor owing to its largest combustor volume. As the axial distance increases, the velocity first rises sharply and then increases slowly with fluctuations as shown in Fig. 19. As the width of the combustor increases, the restriction on the flow

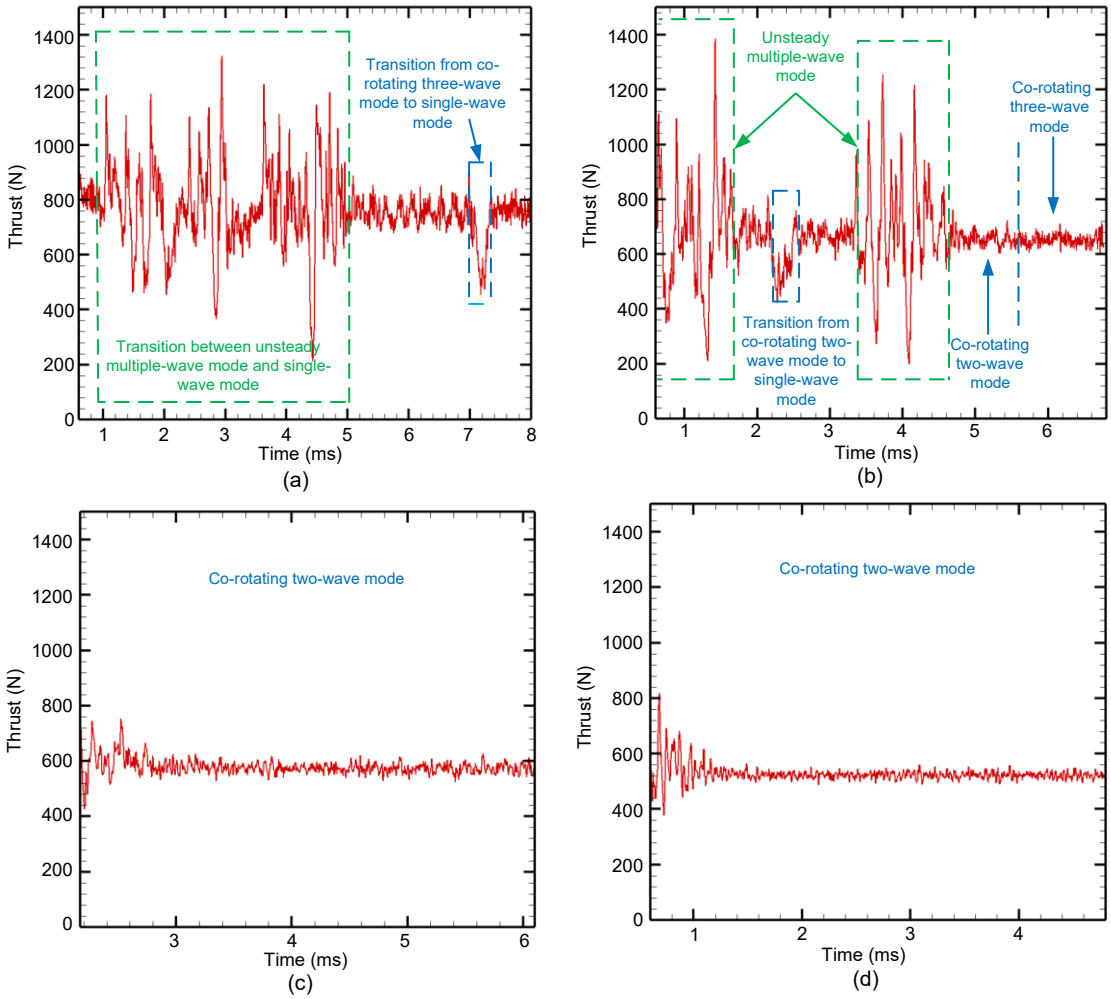

Fig. 17 Thrust record curves of different combustors: (a) W=15 mm; (b) W=20 mm; (c) W=25 mm; (d) W=30 mm

Table 3 Average thrusts and RSDs of thrust of different combustors

W (mm)	Average thrust (N)	RSD (%)
15	758.06	16.92
20	662.03	19.69
25	579.51	5.49
30	525.93	5.87

direction of the combustion product by the inner cylinder decreases. Therefore, the axial velocity decreases as the combustor width increases and results in a great kinetic energy loss in the circumferential and radial directions. This is not conducive to increasing the thrust of the CRDE.

All in all, increasing the width of the combustor is not conducive to increasing the magnitude of the thrust although it is beneficial to improving its stability. Furthermore, enlarging the channel at the forepart of the combustor where the detonation occurs while narrowing the downstream channel where the combustion

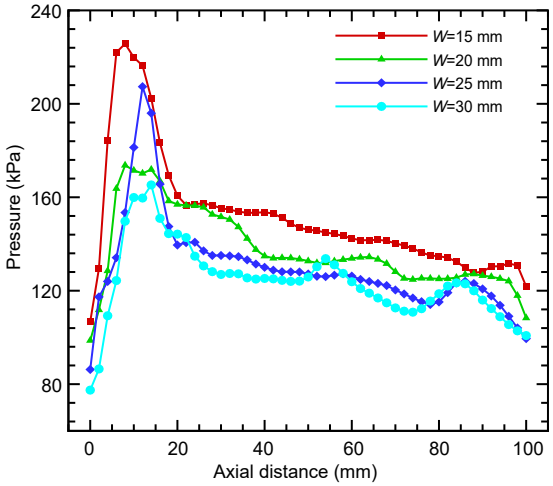

Fig. 18 Mass-average pressures along the axial distance

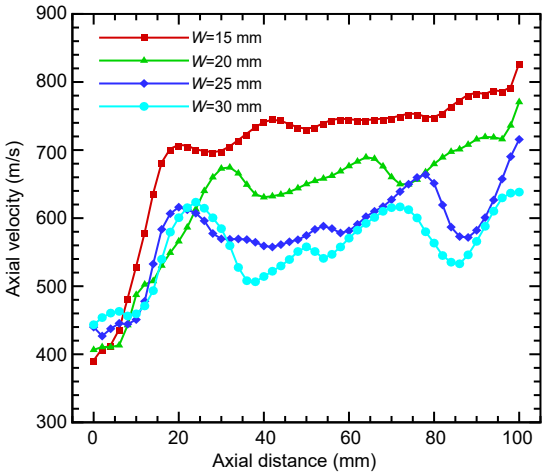

Fig. 19 Mass-average axial velocities along the axial distance

products accelerate may lead to a relatively high and stable thrust of the CRDE. This proposed combustor configuration exactly matches the cavity-based annular combustor.

5 Conclusions

To reveal the impacts of combustor width on the ethylene-air CRD, four cases with different combustor widths are carried out using 3D simulations. Based on the pressure record curves, contours of the flow field, and thrust record curves, simulation results have been analyzed in detail. The main conclusions can be drawn as follows:

1. The critical combustor width to obtain steady propagation of the ethylene-air CRD wave is 25 mm. When the combustor width is smaller than 25 mm, an unsteady multiple-wave mode is observed and the CRD waves do not reach a long-term steady mode. As the combustor width is increased to 25 and 30 mm, the CRD waves can remain steadily and sustainably in a co-rotating two-wave mode.

2. The average propagation velocity of the CRD wave increases as the combustor width is increased. The highest propagation velocity is obtained in the 30-mm wide combustor, reaching 1880.27 m/s, while the lowest propagation velocity is acquired in the 15-mm wide combustor at 1681.01 m/s.

3. A high-temperature zone filled with primary detonation products is observed at the forepart of the wide combustors and its effects are revealed. The high-temperature zone works as a pilot flame and preheats the propellants. This can greatly improve the detonation ability of the propellants and produce chemically active preliminary products.

4. As the combustor width increases, the average thrust of the CRDE decreases while the stability of the thrust increases. With the increase in combustor width, the volume of the combustor increases and the combustion products flow more divergently. This results in a considerable pressure drop in the combustor and great kinetic energy loss in the circumferential and radial directions.

5. The cavity-based annular combustor is supposed to obtain a good propulsive performance of the CRDE. By applying the cavity to the annular combustor, the channel is enlarged at the forepart of the combustor where the detonation occurs, while the downstream channel is narrowed where the combustion products accelerate. This may lead to a relatively high and stable thrust of a CRDE fed by hydrocarbon fuels.

This paper may contribute to understanding the realization mechanism of ethylene-air CRD and enriching the combustor design theory for CRDE. Moreover, how to obtain both steady propagation of the CRD wave and high thrust of the CRDE fed by hydrocarbon fuels is worth further study.

Acknowledgments

This work is supported by the National Natural Science Foundation of China (No. 51776220) and the Postgraduate Scientific Research Innovation Project of Hunan Province, China.

Author contributions

Wei-dong LIU and Hao-yang PENG designed this numerical study. Wei-jie FAN carried out the simulations and analyzed the results under their guidance. Shi-jie LIU and Jian SUN provided important suggestions on the improvement of the simulations. All authors reviewed and revised the manuscript carefully and approved the content of the manuscript.

Conflict of interest

Wei-jie FAN, Wei-dong LIU, Hao-yang PENG, Shi-jie LIU, and Jian SUN declare that they have no conflict of interest.

References

Anand V, George AS, de Luzan CF, et al., 2018. Rotating detonation wave mechanics through ethylene-air mixtures in hollow combustors, and implications to high frequency combustion instabilities. *Experimental Thermal and Fluid*

Science, 92:314-325.
https://doi.org/10.1016/j.expthermflusci.2017.12.004

Andrus IQ, Polanka MD, King PI, et al., 2017. Experimentation of premixed rotating detonation engine using variable slot feed plenum. *Journal of Propulsion and Power*, 33(6):1448-1458.
https://doi.org/10.2514/1.B36261

Baurle RA, Mathur T, Gruber MR, et al., 1998. A numerical and experimental investigation of a scramjet combustor for hypersonic missile applications. Proceedings of the 34th AIAA/ASME/SAE/ASEE Joint Propulsion Conference and Exhibit, p.1-17.
https://doi.org/10.2514/6.1998-3121

Bykovskii FA, Vedernikov EF, 1996. Self-sustaining pulsating detonation of gas-mixture flow. *Combustion, Explosion and Shock Waves*, 32(4):442-448.
https://doi.org/10.1007/BF01998496

Bykovskii FA, Zhdan SA, Vedernikov EF, 2006a. Continuous spin detonation of fuel-air mixtures. *Combustion, Explosion and Shock Waves*, 42(4):463-471.
https://doi.org/10.1007/s10573-006-0076-9

Bykovskii FA, Zhdan SA, Vedernikov EF, 2006b. Continuous spin detonations. *Journal of Propulsion and Power*, 22(6):1204-1216.
https://doi.org/10.2514/1.17656

Bykovskii FA, Vedernikov EF, Polozov SV, et al., 2007. Initiation of detonation in flows of fuel-air mixtures. *Combustion, Explosion, and Shock Waves*, 43(3):345-354.
https://doi.org/10.1007/s10573-007-0048-8

Cho KY, Codoni JR, Rankin BA, et al., 2016. High-repetition-rate chemiluminescence imaging of a rotating detonation engine. Proceedings of the 54th AIAA Aerospace Sciences Meeting, p.1-13.
https://doi.org/10.2514/6.2016-1648

Fan WJ, Zhou J, Liu SJ, et al., 2021. Effects of the geometrical parameters of the injection nozzle on ethylene-air continuous rotating detonation. *Journal of Zhejiang University-SCIENCE A (Applied Physics & Engineering)*, 22(7):547-563.
https://doi.org/10.1631/jzus.A2000314

Fang YS, Hu ZM, Teng HH, et al., 2017. Numerical study of inflow equivalence ratio inhomogeneity on oblique detonation formation in hydrogen–air mixtures. *Aerospace Science and Technology*, 71:256-263.
https://doi.org/10.1016/j.ast.2017.09.027

Fujii J, Kumazawa Y, Matsuo A, et al., 2017. Numerical investigation on detonation velocity in rotating detonation engine chamber. *Proceedings of the Combustion Institute*, 36(2):2665-2672.
https://doi.org/10.1016/j.proci.2016.06.155

George AS, Driscoll RB, Anand V, et al., 2015. Fuel blending as a means to achieve initiation in a rotating detonation engine. Proceedings of the 53rd AIAA Aerospace Sciences Meeting, p.1-18.
https://doi.org/10.2514/6.2015-0633

Gottiparthi KC, Génin F, Srinivasan S, et al., 2009. Simulation of cellular detonation structures in ethylene-oxygen mixtures. Proceedings of the 47th AIAA Aerospace Sciences Meeting Including the New Horizons Forum and Aerospace Exposition, p.1-13.
https://doi.org/10.2514/6.2009-437

Hsu PS, Slipchenko MN, Jiang NB, et al., 2020. Megahertz-rate OH planar laser-induced fluorescence imaging in a rotating detonation combustor. *Optics Letters*, 45(20):5776-5779.
https://doi.org/10.1364/OL.403199

Kawasaki A, Inakawa T, Kasahara J, et al., 2019. Critical condition of inner cylinder radius for sustaining rotating detonation waves in rotating detonation engine thruster. *Proceedings of the Combustion Institute*, 37(3):3461-3469.
https://doi.org/10.1016/j.proci.2018.07.070

Khokhlov AM, Austin JM, Pintgen F, et al., 2004. Numerical study of the detonation wave structure in ethylene-oxygen mixtures. Proceedings of the 42nd AIAA Aerospace Sciences Meeting and Exhibit, p.2-7.
https://doi.org/10.2514/6.2004-792

Kindracki J, 2015. Experimental research on rotating detonation in liquid fuel–gaseous air mixtures. *Aerospace Science and Technology*, 43:445-453.
https://doi.org/10.1016/j.ast.2015.04.006

Le Naour B, Falempin F, Coulon K, 2017. MBDA R&T effort regarding continuous detonation wave engine for propulsion–status in 2016. Proceedings of the 21st AIAA International Space Planes and Hypersonics Technologies Conference, p.1-8.
https://doi.org/10.2514/6.2017-2325

Lin W, Zhou J, Liu SJ, et al., 2015. Experimental study on propagation mode of H_2/air continuously rotating detonation wave. *International Journal of Hydrogen Energy*, 40(4):1980-1993.
https://doi.org/10.1016/j.ijhydene.2014.11.119

Liu SJ, Lin ZY, Liu WD, et al., 2013. Experimental and three-dimensional numerical investigations on H_2/air continuous rotating detonation wave. *Proceedings of the Institution of Mechanical Engineers, Part G: Journal of Aerospace Engineering*, 227(2):326-341.
https://doi.org/10.1177/0954410011433542

Liu SJ, Liu WD, Lin ZY, et al., 2015. Experimental research on the propagation characteristics of continuous rotating detonation wave near the operating boundary. *Combustion Science and Technology*, 187(11):1790-1804.
https://doi.org/10.1080/00102202.2015.1019620

Liu SJ, Peng HY, Liu WD, et al., 2020. Effects of cavity depth on the ethylene-air continuous rotating detonation. *Acta Astronautica*, 166:1-10.
https://doi.org/10.1016/j.actaastro.2019.09.038

Nikitin VF, Dushin VR, Phylippov YG, et al., 2009. Pulse detonation engines: technical approaches. *Acta Astronautica*, 64(2-3):281-287.
https://doi.org/10.1016/j.actaastro.2008.08.002

Peng HY, Liu WD, Liu SJ, et al., 2018. Experimental investigations on ethylene-air continuous rotating detonation wave in the hollow chamber with Laval nozzle. *Acta Astronautica*, 151:137-145.
https://doi.org/10.1016/j.actaastro.2018.06.025

Peng HY, Liu WD, Liu SJ, et al., 2019a. The effect of cavity

on ethylene-air continuous rotating detonation in the annular combustor. *International Journal of Hydrogen Energy*, 44(26):14032-14043. https://doi.org/10.1016/j.ijhydene.2019.04.017

Peng HY, Liu WD, Liu SJ, 2019b. Ethylene continuous rotating detonation in optically accessible racetrack-like combustor. *Combustion Science and Technology*, 191(4):676-695. https://doi.org/10.1080/00102202.2018.1498850

Peng HY, Liu WD, Liu SJ, et al., 2021. Effects of cavity location on ethylene–air continuous rotating detonation in a cavity-based annular combustor. *Combustion Science and Technology*, 193(16):2761-2782. https://doi.org/10.1080/00102202.2020.1760255

Schwer D, Kailasanath K, 2013. Fluid dynamics of rotating detonation engines with hydrogen and hydrocarbon fuels. *Proceedings of the Combustion Institute*, 34(2):1991-1998. https://doi.org/10.1016/j.proci.2012.05.046

Schwer DA, Kailasanath K, 2012. Feedback into mixture plenums in rotating detonation engines. Proceedings of the 50th AIAA Aerospace Sciences Meeting Including the New Horizons Forum and Aerospace Exposition, p.1-17. https://doi.org/10.2514/6.2012-617

Stewart DS, Kasimov AR, 2006. State of detonation stability theory and its application to propulsion. *Journal of Propulsion and Power*, 22(6):1230-1244. https://doi.org/10.2514/1.21586

Sun J, Zhou J, Liu SJ, et al., 2017. Effects of injection nozzle exit width on rotating detonation engine. *Acta Astronautica*, 140:388-401. https://doi.org/10.1016/j.actaastro.2017.09.008

Sun J, Zhou J, Liu SJ, et al., 2018a. Numerical investigation of a rotating detonation engine under premixed/non-premixed conditions. *Acta Astronautica*, 152:630-638. https://doi.org/10.1016/j.actaastro.2018.09.012

Sun J, Zhou J, Liu SJ, et al., 2018b. Plume flowfield and propulsive performance analysis of a rotating detonation engine. *Aerospace Science and Technology*, 81:383-393. https://doi.org/10.1016/j.ast.2018.08.024

Sun J, Zhou J, Liu SJ, et al., 2019. Interaction between rotating detonation wave propagation and reactant mixing. *Acta Astronautica*, 164:197-203. https://doi.org/10.1016/j.actaastro.2019.08.010

Tang XM, Wang JP, Shao YT, 2015. Three-dimensional numerical investigations of the rotating detonation engine with a hollow combustor. *Combustion and Flame*, 162(4):997-1008. https://doi.org/10.1016/j.combustflame.2014.09.023

Wang YH, Le JL, Wang C, et al., 2018. A non-premixed rotating detonation engine using ethylene and air. *Applied Thermal Engineering*, 137:749-757. https://doi.org/10.1016/j.applthermaleng.2018.04.015

Wilhite J, Driscoll R, George AS, et al., 2016. Investigation of a rotating detonation engine using ethylene-air mixtures. Proceedings of the 54th AIAA Aerospace Sciences Meeting, p.1-7. https://doi.org/10.2514/6.2016-1650

Yang CL, Wu XS, Ma H, et al., 2016. Experimental research on initiation characteristics of a rotating detonation engine. *Experimental Thermal and Fluid Science*, 71:154-163. https://doi.org/10.1016/j.expthermflusci.2015.10.019

Yao SB, Tang XM, Wang JP, 2017. Numerical study of the propulsive performance of the hollow rotating detonation engine with a Laval nozzle. *International Journal of Turbo & Jet-Engines*, 34(1):49-54. https://doi.org/10.1515/tjj-2015-0052

Yi TH, Lou J, Turangan C, et al., 2011. Propulsive performance of a continuously rotating detonation engine. *Journal of Propulsion and Power*, 27(1):171-181. https://doi.org/10.2514/1.46686

Yungster S, Radhakrishnan K, 2005. Structure and stability of one-dimensional detonations in ethylene-air mixtures. *Shock Waves*, 14(1):61-72. https://doi.org/10.1007/s00193-005-0242-0